PREPRINT version
Short Photoluminescence Lifetimes in Vacuum-Deposited $CH_3NH_3PbI_3$ Perovskite Thin Films as a Result of Fast Diffusion of Photogenerated Charge Carriers

Vladimir S. Chirvony,*,†,‡ Kairolla S. Sekerbayev,§ Daniel Pe´rez-del-Rey,† Juan P. Martínez-Pastor,‡ Francisco Palazon,† Pablo P. Boix,† Toktar I. Taurbayev,§ Michele Sessolo,† and Henk J. Bolink†

†Instituto de Ciencia Molecular, Universidad de Valencia, c/Catedra´tico J. Beltra´n, 2, Paterna 4698, Spain
‡UMDO (Unidad de Materiales y Dispositivos Optoelectro´nicos), Instituto de Ciencia de los Materiales, Universidad de Valencia,
Valencia 46071, Spain
§Institute of Experimental and Theoretical Physics, Al-Farabi Kazakh National University, Almaty 050040, Kazakhstan

ABSTRACT: It is widely accepted that a long photoluminescence (PL) lifetime in metal halide perovskite films is a crucial and favorable factor, as it ensures a large charge diffusion length leading to a high power conversion efficiency (PCE) in solar cells. It has been recently found that vacuumevaporated $CH_3NH_3PbI_3$ (eMAPI) films show very short PL lifetimes of several nanoseconds. The corresponding solar cells, however, have high photovoltage (>1.1 V) and PCEs (up to 20%). We rationalize this apparent contradiction and show that eMAPI films are characterized by a very high diffusion coefficient D, estimated from modeling the PL kinetics to exceed 1 cm^2/s. Such high D values are favorable for long diffusion length as well as fast transport of carriers to film surfaces, where they recombine nonradiatively with surface recombination velocity $S \sim 10^4$ cm/s. Possible physical origins leading to the high D values are also discussed

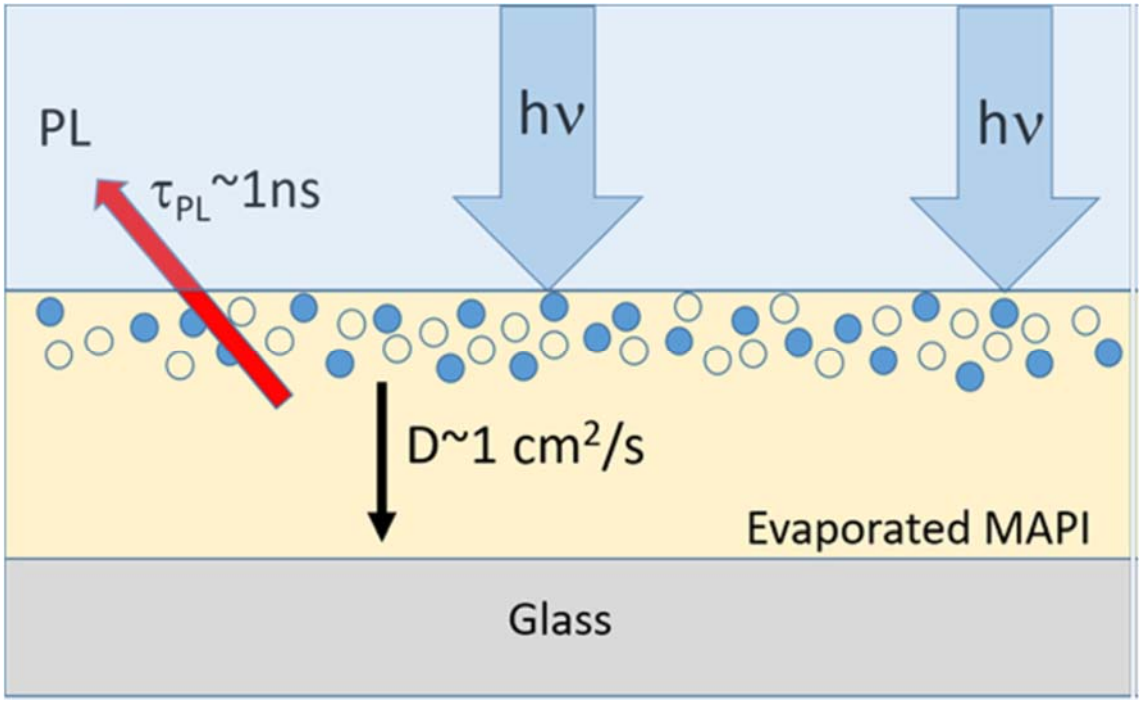

The widespread research toward solution-processing technologies for the fabrication of solar cells based on metal halide perovskites (hereinafter perovskites) resulted in the fast progress in power conversion efficiencies (PCE) of the devices, from 3.8% in 2009[1] to 23.7% in 2019.[2] One of the most important parameters of a photovoltaic material is the diffusion length L_D of the photogenerated charge carriers. For efficient carrier transport in a solar cell, L_D has to be sufficiently long and exceed the absorption length and thickness of the active layer. Perovskites show diffusion lengths ranging from 100 nm for polycrystalline films,[3] to hundreds of micrometers in the case of single crystals.[4,5] The carrier lifetime τ is considered to be the main factor determining the diffusion lengths in perovskite films, according to the expression $L_D = \sqrt{D\tau}$ where D is the diffusion coefficient (diffusivity) and τ is the carrier recombination lifetime.

For solution processed, unpassivated polycrystalline perovskite films, τ usually exceeds a hundred of nanoseconds, as measured by the photoluminescence (PL) decay kinetics.[6−8] However, extremely short PL lifetimes (several nanoseconds) have been recently reported for polycrystalline methylammonium lead iodide films produced by vacuum evaporation/deposition (hereinafter eMAPI).[9−11] In spite of such short PL lifetimes, the PCE of the vacuum-deposited solar cells is similar to those obtained with solution-processed MAPI layers (hereinafter sMAPI)[12,13] which usually exhibit PL lifetimes on the time scale of hundreds of nanoseconds. As was previously noted this observation is in apparent contradiction with the hypothesis assigning a leading role to long carrier lifetimes in obtaining high L_D (and therefore PCE).

In the present work we investigate PL transients of eMAPI layers on glass and demonstrate that, at charge carrier concentrations compatible with solar illumination (10^{15}−10^{16} cm^{-3}), at which the contribution of the radiative band-to-band recombination is negligible, the short PL kinetics originates from the fast carrier diffusion followed by nonradiative recombination at the layer surfaces. This finding allowed usto apply the one-dimentional diffusion equation to model the PL kinetics and to determine the ambipolar diffusion coefficient D and the surface recombination velocity S. We found that in the case of eMAPI the diffusivity D exceeds 1 cm^2/s, which is more than 1 order of magnitude higher than average values observed for sMAPI films. At the same time, the fitting disclosed also high values of the surface recombination velocity $S \sim 10^4$ cm/s. The obtained values of the diffusion coefficient are close to the maximum values of D known in the literature for both polycrystalline layers and single crystals of perovskites.

Preparation of eMAPI films, deposition of passivating layers as well as fabrication of the corresponding solar cells was carried out in a nitrogen atmosphere, as described in detail in the Materials and Methods (see Supporting Informatiom). To study the effect of passivation and to minimize any possible sample-to-sample variation, 3 × 3 cm^2 eMAPI coated glass slides were cut into nine 1 cm^2 samples. Some of these were analyzed without further treatment; others were coated with a thin (<20 nm) layer of trioctylphosphine oxide (TOPO) as the passivating agent.[14] Investigation of the PL transients for pristine and passivated eMAPI films on glass was carried out at room temperature in air for 2−3 h after sample preparation. During this time neither the PL kinetics nor the spectral shape varied.

Figure 1 shows photovoltaic characteristics of solar cells fabricated using eMAPI layers of three different thicknesses. In the case of 600 and 970 nm thick absorbers, the PCE was as high as 19.9 and 20.6%, similar to the previously reported best vacuum-deposited and solution-processed perovskite solar cells using MAPI as the active material.[12,15] Of particular interest is the open circuit voltage (V_{oc}), which is basically thicknessindependent and as high as 1.16 V for a 1 μm thick eMAPI perovskite film. This is indicative of a high quality semiconductor, where bulk nonradiative recombination is almost suppressed. Nevertheless, despite the high performance of the solar cells, the PL transients of freshly prepared eMAPI layers on glass are very short (not longer than several nanoseconds; see a representative PL transient in Figure 2a) as compared to the PL lifetimes typically reported for sMAPI films.[6−8] Such unusually short PL lifetimes were highlighted in several earlier publications.[9−11] In the framework of the commonly accepted recombination scheme for perovskites,[16,17] the short PL lifetimes in eMAPI could be explained by the presence of efficient nonradiative bulk recombination. However, this would imply recombination losses that are inconsistent with the high PCE and especially the high open circuit voltage we found in solar cells (Figure 1). Short PL lifetimes in eMAPI films have been attributed to the high contribution of the radiative bandto- band recombination to the PL kinetics.[11] In turn, we assume that the observed short carrier lifetimes are caused by nonradiative recombination on the perovskite surface but not in bulk. In this scenario, the PL decay kinetics in eMAPI should strongly lengthen after surface passivation.[14,18]

To test this idea, we used TOPO as a well-known surface passivating agent.[14,18] Typical PL transients measured for eMAPI layers before and after passivation of their front surface by TOPO are shown in Figure 2 (excitation by 100 fs light pulses at 405 nm with a pulse repetition rate of 76 MHz). The nonpassivated eMAPI layer demonstrated short PL decay kinetics (symbols in Figure 2a and in Figure 2b, curve 1), which is well described by a monoexponentially decaying function (the exponential modeling is not shown) with a time constant of 0.75 ns. After passivation by TOPO, the sample showed much longer kinetics (symbols in Figure 2b, curve 2), which is also well described by a monoexponentially decaying function, but with a much longer time constant of τ_{PL} = 73.5 ns. Note that in the case of the passivated layer, due to the small time interval T (13 ns) between successive excitation pulses, the condition $T < \tau_{PL}$ is fulfilled, so that only part of the PL decay kinetics is experimentally recorded. However, we demonstrate below by numerical modeling of carrier diffusion processes initiated by single and repetitive pulse excitation that the initial 13 ns part of the ~100 ns decay kinetics has the same decay time constant as the full kinetics obtained after single-pulse excitation (Figure 2c and corresponding text). Thus, the passivation of only one (front) surface of eMAPI layer leads to a lengthening of the experimentally observed PL lifetime τ_{PL} from ~1 ns to ~100 ns. This fact clearly indicates that (i) the PL decay kinetics of the nonpassivated layer is strongly determined by carrier surface recombination and (ii) the bulk carrier lifetime τ_B is equal to or longer than ~100 ns.

Literature data obtained for TOPO-passivated solutionprepared MAPI layers demonstrate that τ_B has a magnitude of the order of 1 μs or more,[14,18] but for our further calculations and evaluations we will assume that $\tau_B = \tau_{PL} \sim 100$ ns. As discussed below, the impact of the bulk lifetime value (whereas τ_B is 100 or 1000 ns) on our numerical analysis of PL transients in nonpassivated eMAPI layer is negligible, as the condition $\tau_{PL} \ll \tau_B$ is satisfied anyway.

The simulation of carrier diffusion in thin film semiconductors is facilitated by the fact that the diffusion of carriers occurs only orthogonally to the sample surface (defined by the light incidence). Indeed, due to the large absorption coefficient α at the excitation wavelength ($\alpha_{405} = 1.5 \times 10^5$ cm^{-1} in our case), all the light is absorbed within less than 100 nm thickness, where free carriers are formed. As a result, carrier diffusion occurs, which is directed along the carrier concentration gradient, and hence is perpendicular to the surface of the layer. To describe the carrier diffusion process, we use a one-dimensional diffusion eq 1 under the assumption that the kinetics of the carrier concentration decay is described only by two nonradiative recombination processes, which are linear with respect to the concentration n: (i) surface recombination (see boundary conditions below) and (ii) bulk recombination (described by the second

$$\frac{\partial n(x,t)}{\partial t} = D\frac{\partial^2 n(x,t)}{\partial x^2} - \frac{n(x,t)}{\tau_B} + G(x,t)$$

where D is the diffusion coefficient, τ_B is the bulk carrier lifetime (set to 100 ns in our case), and G(x,t) is the generation rate upon a light pulse. We intentionally did not include in eq 1 a term proportional to n^2, corresponding to the radiative bimolecular recombination, since its presence reduces the reproducibility and accuracy of fitting the experimental kinetics. This circumstance requires, however, that experimental measurements of the PL transients are performed at low concentrations of photoexcited carriers, when the quadratic term can be neglected (see Note 1 in the Supporting Information). We consider two excitation regimes: single pulse excitation and repetitive pulse excitation. In the former case the concentration of excited carriers at the initial time is assumed to be zero:

In the case of repetitive excitation with the time interval T between pulses we consistently calculated each excitation cycle.

The initial value of the concentration of the next calculation cycle is taken as the final value of the previous one. In this case, condition 2a is modified as follows:

$= - n_i(x,0)\ n_{i\,1}(x,T)$ (2b) where T = 13 ns and i is the cycle number. The cycles are calculated until an equilibrium is established, i.e., when the carrier concentration profile does not change when calculating a new cycle. The number of photogenerated charge carriers is proportional to the intensity of the excitation signal:

$\propto \cdot {}^{-\alpha} G(x,t)\, I(x,t)\, e^{x}$ (3)

where α is the absorption coefficient at the excitation wavelength, and the excitation signal profile I(x,t) is modeled by the Gaussian distribution $\propto {}^{-[-\mu]}\, I(x,t)\, e^{4(t)/w \ln 2\, 2\, 2}$ where w is the excitation pulse half width and μ is a position of the excitation pulse maximum. We used also standard boundary conditions describing recombination on the front (eq 4) and rear (eq 5) surfaces of the layer:

$$\left.\frac{\partial n(x,t)}{\partial x}\right|_{x=0} = \frac{S_F}{D} n(0,t) \qquad (4$$

$$\left.\frac{\partial n(x,t)}{\partial x}\right|_{x=L} = -\frac{S_B}{D} n(d,t) \qquad (5$$

where S_F and S_B are the surface recombination velocity on the front and back side, respectively, and d is the layer thickness. The numerical solution of the differential equation was made in the framework of the Crank−Nicolson difference scheme. The relationship between the distribution of charge carriers over the layer thickness and the experimentally measured kinetics of the PL decay $I_{PL}(t)$ is given by the following equation:

$$I_{PL}(t) = \int_0^L n(x,t)\, dx \qquad (6)$$

In (6), only monomolecular (both bulk and surface) carrier recombination was taken into account, in accordance with our requirement to work at sufficiently low n to prevent bimolecular processes. Our estimates show that the maximum permissible n, which still enables to avoid bimolecular recombination, depends on the PL transient lifetime and is ~10^{17} cm^{-3} for transients with τ_{PL} ~ 1 ns and ~ 10^{15} cm^{-3} for transients with τ_{PL} ~ 100 ns (see Note 1 in the Supporting Information). Importantly, the carrier concentration range of 10^{15}−10^{16} cm^{-3} corresponds to the characteristic concentrations in perovskite solar cells under 1 sun illumination.[19]

The results of fitting of the experimental PL transients of nonpassivated eMAPI by the diffusion equation (1) are shown in Figure 2a (solid line). The fitting allows one to determine simultaneously the values of the diffusion coefficient D and the surface recombination velocity S. In the case of nonpassivated eMAPI layer we assume $S_F = S_B = S$. In the case of the frontpassivated layer we assume $= + S\, S\, S$ eff 2 F B (we cannot evaluate separately S_F and S_B because we are not able to passivate the buried interface of the layer). It turned out that for the nonpassivated eMAPI layer, the fitting procedure enables us to determine only the lower limit of the diffusion coefficient due to very high values of D. The best fitting to experimental

results shown in Figure 2a was obtained by using D ≥ 1.0 cm^2/ s and S = 4.5 × 10^4 cm/s. The PL kinetics modeling by the diffusion equation presented in Figure S2a demonstrates how, at high D values, the kinetics becomes insensitive to D. Apart from the PL kinetics for nonpassivated eMAPI, we modeled also the carrier concentration distribution over the layer thickness as a function of time (see Figure S2b). As one can see, immediately after excitation, photogenerated carriers become homogeneously distributed over the film thickness.

We believe that this fast carrier redistribution over the full layer thickness is why, after passivation of the eMAPI layer front side, the PL lifetime increases only to ~100 ns but not to ~1 μs as in the case of sMAPI layers. Indeed, in the case of sMAPI, for which D is usually ≪1 cm^2/s, the carrier redistribution is much slower so that the back side practically does not participate in photoexcited carrier quenching (Figure S2c). In order to fit long-lived PL transients observed for passivated eMAPI films (curve 2 in Figure 2b), we have developed a different procedure that enables us to model the PL response when T < τ_{PL}. The fitting results in S_{eff} = 120 cm/ s at τ_B = 100 ns. We suggest here

D = 1.0 cm^2/s, as in the case of nonpassivated layers, because passivation by TOPO is a surface effect and should not change the perovskite bulk properties.[18] When $T < \tau_{PL}$, photoexcited carriers do not recombine completely between consecutive excitation pulses, so that ~80% of the PL signal is from permanently excited carriers and only ~20% corresponds to the signal decaying between pulses (Figure 2b). It is interesting to note that the model developed for the regime of high repetition rate excitation enabled us to vizualize how the PL background arises after first excitation pulses and then saturates. It turned out that the stationary mode is set during about 200 ns after starting the excitation in the case of our TOPO-saturated layer, which corresponds to less than 20 excitation pulses (see Note 2 and Figure S3).

To ensure that the fitting procedure correctly reproduces the PL decay of the layer over the 13 ns window of the high repetition rate kinetics, we additionally simulated the same PL decay kinetics (i.e., using D = 1 cm^2/s, S = 120 cm/s, τ_B = 100 ns, $\alpha_{405} = 1.5 \times 10^5$ cm^{-1}) under single-pulse excitation regime. As can be seen from Figure 2c, both kinetics lead to the same decay time constant of 73.5 ns. The absence of the contribution of bimolecular recombination under excitation conditions in our experiment ($n \sim 10^{15}$ cm^{-3}) is confirmed by the fact that the PL transient practically does not change with a further decrease of the excitation intensity.

An analysis of the literature data on experimentally measured values of D for perovskite polycrystalline layers and single crystals allows us to propose some hypothesis about the origin of fast diffusion in eMAPI layers, that we and other authors have discovered. We have to note first of all that the reported D values for MAPI polycrystalline films prepared by spincoating spread in a wide range, from 10^{-5} to 2.7 cm^2/s,[3,20−33] with the most common values ranging from 0.01 to 0.1 cm^2/s.[3,32] Such a large scattering of results is partly due to differences in the perovskite layer preparation and properties.

However, an important factor to be considered is also the type of measurement used to estimate the diffusion coefficient D (or the associated carrier mobility μ), and if such a method investigates the short- or long-range carrier transport.[34] Indeed, average carrier mobility for MAPI films measured by terahertz and microwave conductivity (short-range methods, giving information about carrier transport at the submicrometer scale), is 37 $cm^2/(V\ s)$ (D = 0.93 cm^2/s). This is rather similar to the average values of μ = 73 $cm^2/(V\ s)$ (D = 1.8 cm^2/s) found for MAPI single crystals.[34] Besides, recent direct measurements of D by the light induced transient grating method also showed that the diffusion coefficient of carriers, in the plane of the layer at distances shorter than the grain size, is of the same order of 1−2 cm^2/s.[35,36] Thus, it is reasonable to assume that the transport of carriers within individual perovskite grains in polycrystalline films and in the volume of single crystals is rather similar, with a diffusion coefficient within ~1−2 cm^2/s.

The transient PL method provides information about the long-range charge transport, giving an average diffusivity value over the whole layer thickness (i.e., along the entire path of the carrier diffusion).[34] Since our transient PL method yields high D values for eMAPI layers, we suggest that the film might be composed by perovskite grains growing through its entire thickness. In this way, diffusion would occur across the layer as in a perovskite single crystal, justifying the large diffusivity observed here.[34,37,38] Future studies will be focused on the task to resolve structurally the morphology of our eMAPI films. Also, it is worthwhile to discuss how the high values of the surface recombination velocity ($S \sim 10^4$ cm/s) of nonpassivated eMAPI might still be compatible with the high efficiency of the corresponding solar cells, especially in view of much lower S reported for polycrystalline sMAPI ($S = 0.45 \times 10^3$ cm/s) and MAPI single crystals ($S = 2.8 \times 10^3$ cm/s).[39] This apparent contradiction can be rationalized considering that in solar cells, the transport layers applied to the perovskite surfaces can efficiently passivate them.[40]

In conclusion, our analysis shows that the perovskite layer PL lifetime cannot be used as the sole indicator predicting the efficiency of the corresponding solar cells. We have demonstrated that in thin eMAPI films under photogenerated carrier concentrations comparable with solar irradiation, the diffusion coefficient D reaches values exceeding 1 cm^2/s. Such high D values provide a very fast (several ns) delivery of charges to both film surfaces where, in the case of nonpassivated perovskite, nonradiative recombination take place. Therefore, the observed short recombination time is notan obstacle to obtain sufficiently long diffusion lengths. Indeed, following the formula $L_D = \sqrt{D\tau_B}$, the diffusion length L_D can be as long as 3−10 μm for τ_B between 100 ns to 1 μs.

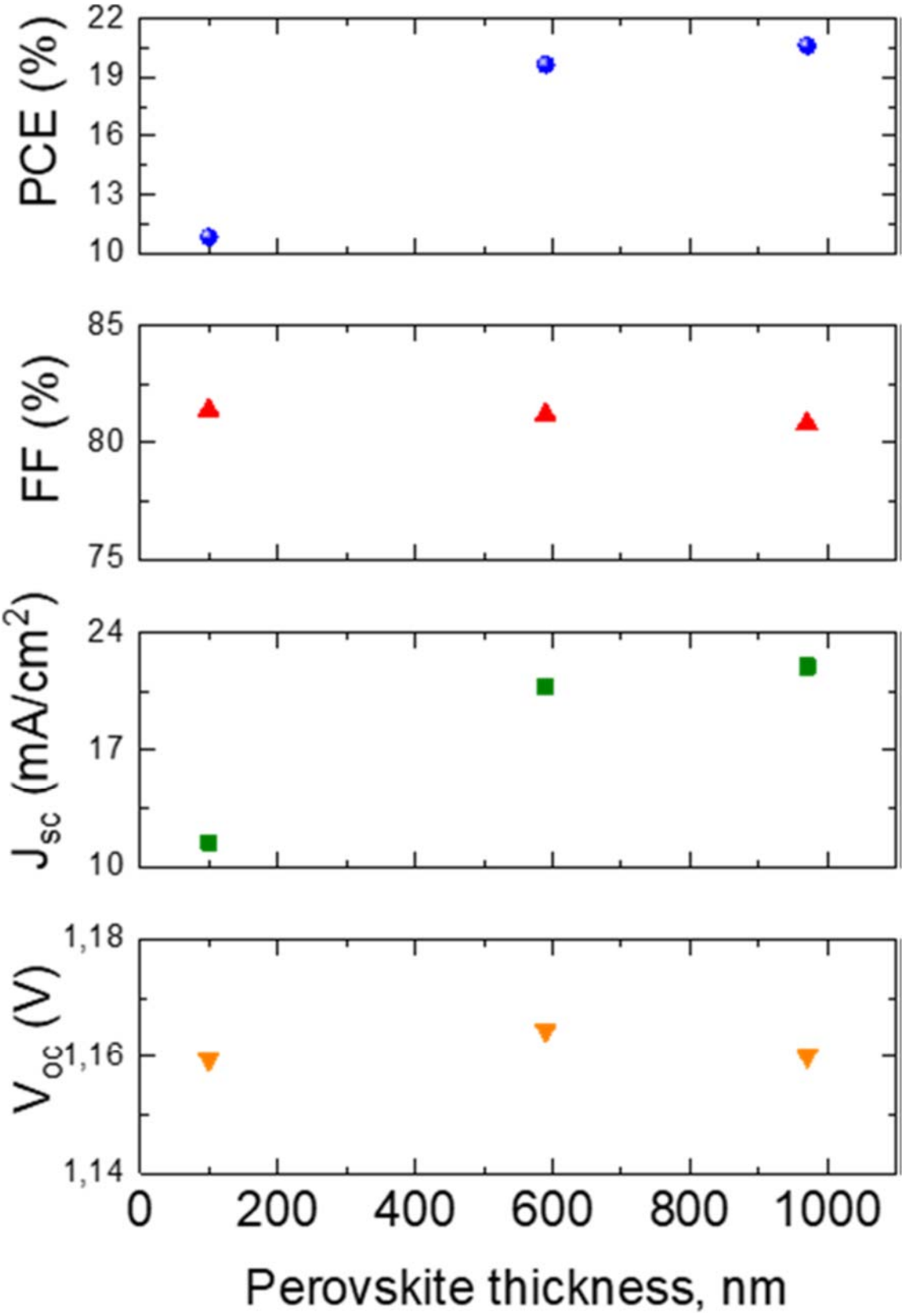

Figure 1. Photovoltaic parameters of vacuum deposited solar cells using eMAPI films with 100, 600, and 970 nm thickness.

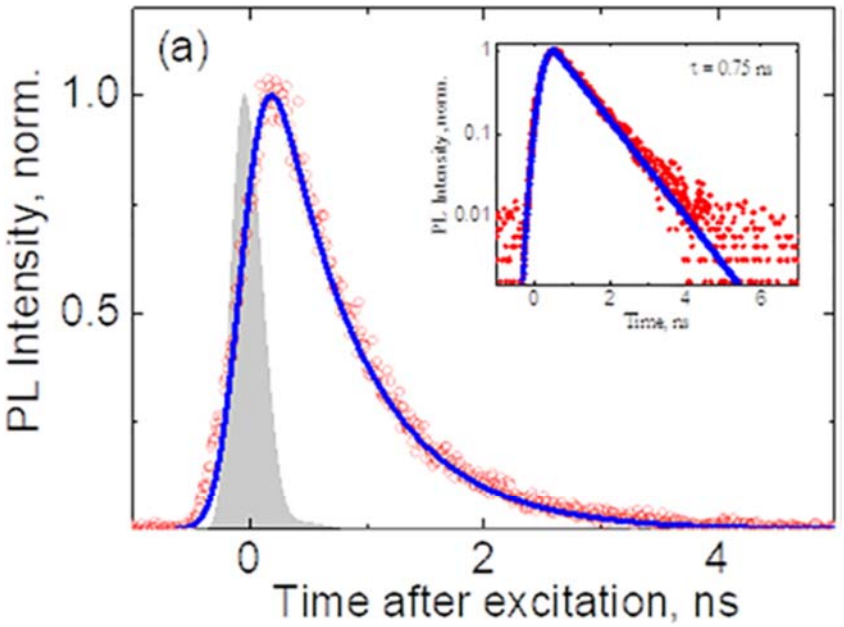
(a)
PL Intensity, norm.
1.0
0.5
0
2
4
Time after excitation, ns
τ = 0.75 ns
PL Intensity, norm.
1
0.1
0.01
0
2
4
6
Time, ns

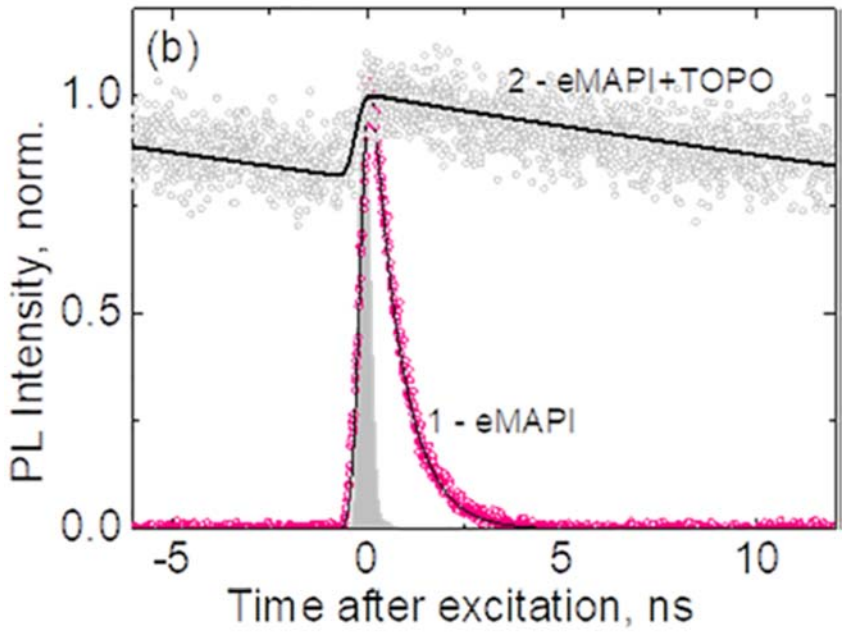
(b)
2 - eMAPI+TOPO
1 - eMAPI
PL Intensity, norm.
1.0
0.5
0.0
-5
0
5
10
Time after excitation, ns

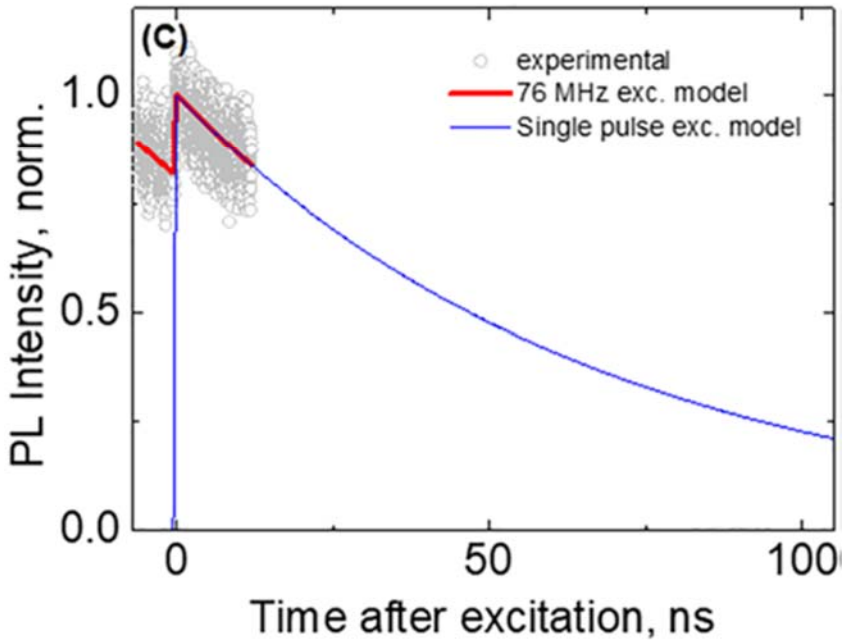
(c)
experimental
76 MHz exc. model
Single pulse exc. model
PL Intensity, norm.
1.0
0.5
0.0
0
50
100
Time after excitation, ns

Figure 2. Experimental (symbols) and model (solid lines) PL transients determined for 500 nm thick eMAPI layer on glass in the case of a nonpassivated [(a) and curve 1 in (b)] and TOPOpassivated [curve 2 in (b) and (c)] layers. The inset in (a) is the same PL transient but plotted in log scale. Comparison of the transients obtained by periodic excitation with time interval 13 ns between pulses (solid red line) with that obtained by a single pulse excitation (solid blue line) is presented in (c)

ORCID
Vladimir S. Chirvony: 0000-0003-4121-9773
Francisco Palazon: 0000-0002-1503-5965
Pablo P. Boix: 0000-0001-9518-7549
Michele Sessolo: 0000-0002-9189-3005
Henk J. Bolink: 0000-0001-9784-6253

Notes

The authors declare no competing financial interest.

ACKNOWLEDGMENTS

The research leading to these results has received funding from the European Union Programme for Research and Innovation Horizon 2020 (2014−2020) under the Marie Skłodowska-Curie Grant Agreement PerovSAMs No. 747599, from the European SOLARERA.NET through the project HIPER, from the Spanish Ministry of Economy and Competitiveness (MINECO) via the Unidad de Excelencia Mari´a de Maeztu MDM-2015-0538 and via the projects MAT2017-88821-R, PCIN-2015-255, PCIN-2017-014, and TEC2017-86102-C2-1-R, and from the Generalitat Valenciana (Prometeo/2016/135). P.B. and M.S. thank the MINECO for their RyC contracts. P.B. acknowledges the financial support from the Conselleria d'Educacio´, Investigacio´, Cultura i Esport Valenciana (SEJI2017/2017/012).

REFERENCES

(1) Kojima, A.; Teshima, K.; Shirai, Y.; Miyasaka, T. Organometal Halide Perovskites as Visible-Light Sensitizers for Photovoltaic Cells. J. Am. Chem. Soc. 2009, 131, 6050−6051.

(2) Green, M. A.; Hishikawa, Y.; Dunlop, E. D.; Levi, D. H.; Hohl-Ebinger, J.; Yoshita, M.; Ho-Baillie, A. W. Y. Solar Cell Efficiency Tables (Version 53). Prog. Photovoltaics 2019, 27, 3−12.

(3) Stranks, S. D.; Eperon, G. E.; Grancini, G.; Menelaou, C.; Alcocer, M. J. P.; Leijtens, T.; Herz, L. M.; Petrozza, A.; Snaith, H. J. Electron-Hole Diffusion Lengths Exceeding 1 Micrometer in an Organometal Trihalide Perovskite Absorber. Science 2013, 342, 341−344.

(4) Dong, Q.; Fang, Y.; Shao, Y.; Mulligan, P.; Qiu, J.; Cao, L.; Huang, J. Electron-Hole Diffusion Lengths > 175 μm in Solution-Grown $CH_3NH_3PbI_3$ Single Crystals. Science 2015, 347, 967−970.

(5) Zhang, F.; Yang, B.; Li, Y.; Deng, W.; He, R. Extra Long Electron-Hole Diffusion Lengths in $CH_3NH_3PbI_{3-x}Cl_x$ Perovskite Single Crystals. J. Mater. Chem. C 2017, 5, 8431−8435.

(6) Eperon, G. E.; Stranks, S. D.; Menelaou, C.; Johnston, M. B.; Herz, L. M.; Snaith, H. J. Formamidinium Lead Trihalide: a Broadly Tunable Perovskite for Efficient Planar Heterojunction Solar Cells. Energy Environ. Sci. 2014, 7, 982−988.
(7) Pellet, N.; Gao, P.; Gregori, G.; Yang, T.-Y.; Nazeeruddin, M. K.; Maier, J.; Gra¨tzel, M. Mixed-Organic-Cation Perovskite Photovoltaics for Enhanced Solar-Light Harvesting. Angew. Chem., Int. Ed. 2014, 53, 3151−3157.
(8) Rehman, W.; Milot, R. L.; Eperon, G. E.; Wehrenfennig, C.; Boland, J. L.; Snaith, H. J.; Johnston, M. B.; Herz, L. M. Charge-Carrier Dynamics and Mobilities in Formamidinium Lead Mixed-Halide Perovskites. Adv. Mater. 2015, 27, 7938−7944.
(9) Patel, J. B.; Milot, R. L.; Wright, A. D.; Herz, L. M.; Johnston, M. B. Formation Dynamics of $CH_3NH_3PbI_3$ Perovskite Following Two Step Layer Deposition. J. Phys. Chem. Lett. 2016, 7, 96−102.
(10) Borchert, J.; Milot, R. L.; Patel, J. B.; Davies, C. L.; Wright, A. D.; Martínez Maestro, L.; Snaith, H. J.; Herz, L. M.; Johnston, M. B. Large-Area, Highly Uniform Evaporated Formamidinium Lead Triiodide Thin Films for Solar Cells. ACS Energy Lett. 2017, 2, 2799−2804.
(11) Levine, I.; Gupta, S.; Bera, A.; Ceratti, D.; Hodes, G.; Cahen, D.; Guo, D.; Savenije, T. J.; A´vila, J.; Bolink, H. J.; et al. Can. We Use Time-Resolved Measurements to Get Steady-State Transport Data for Halide Perovskites? J. Appl. Phys. 2018, 124, 103103.
(12) Momblona, C.; Gil-Escrig, L.; Bandiello, E.; Hutter, E. M.; Sessolo, M.; Lederer, K.; Blochwitz-Nimoth, J.; Bolink, H. J. Efficient Vacuum Deposited p-i-n and n-i-p Perovskite Solar Cells Employing Doped Charge Transport Layers. Energy Environ. Sci. 2016, 9, 3456−3463.
(13) Pe´rez-del-Rey, D.; Boix, P. P.; Sessolo, M.; Hadipour, A.; Bolink, H. J. Interfacial Modification for High-Efficiency Vapor-Phase-Deposited Perovskite Solar Cells Based on a Metal Oxide Buffer Layer. J. Phys. Chem. Lett. 2018, 9, 1041−1046.
(14) Braly, I. L.; deQuilettes, D. W.; Pazos-Outo´n , L. M.; Burke, S.; Ziffer, M. E.; Ginger, D. S.; Hillhouse, H. W. Hybrid Perovskite Films Approaching the Radiative Limit with Over 90% Photoluminescence Quantum Efficiency. Nat. Photonics 2018, 12, 355−361.
(15) Stolterfoht, M.; Wolff, C. M.; Ma´rquez, J. A.; Zhang, S.; Hages, C. J.; Rothhardt, D.; Albrecht, S.; Burn, P. L.; Meredith, P.; Unold, T.; et al. Visualization and Suppression of Interfacial Recombination for High-Efficiency Large-Area pin Perovskite Solar Cells. Nat. Energy 2018, 3, 847−854.
(16) Stranks, S. D.; Burlakov, V. M.; Leijtens, T.; Ball, J. M.; Goriely, A.; Snaith, H. J. Recombination Kinetics in Organic-Inorganic Perovskites: Excitons, Free Charge, and Subgap States. Phys. Rev. Appl. 2014, 2, 034007.
(17) Yamada, Y.; Nakamura, T.; Endo, M.; Wakamiya, A.; Kanemitsu, Y. Photocarrier Recombination Dynamics in Perovskite $CH_3NH_3PbI_3$ for Solar Cell Applications. J. Am. Chem. Soc. 2014, 136, 11610−11613.
(18) deQuilettes, D. W.; Koch, S.; Burke, S.; Paranji, R. K.; Shropshire, A. J.; Ziffer, M. E.; Ginger, D. S. Photoluminescence Lifetimes Exceeding 8 μs and Quantum Yields Exceeding 30% in Hybrid Perovskite Thin Films by Ligand Passivation. ACS Energy Lett. 2016, 1, 438−444.
(19) Wheeler, S.; Bryant, D.; Troughton, J.; Kirchartz, T.; Watson, T.; Nelson, J.; Durrant, J. R. Transient Optoelectronic Analysis of the Impact of Material Energetics and Recombination Kinetics on the Open-Circuit Voltage of Hybrid Perovskite Solar Cells. J. Phys. Chem. C 2017, 121, 13496−13506.

(20) Chen, Y.; Peng, J.; Su, D.; Chen, X.; Liang, Z. Efficient and Balanced Charge Transport Revealed in Planar Perovskite Solar Cells. ACS Appl. Mater. Interfaces 2015, 7, 4471−4475.
(21) Maynard, B.; Long, Q.; Schiff, E. A.; Yang, M.; Zhu, K.; Kottokkaran, R.; Abbas, H.; Dalal, V. L. Electron and Hole Drift Mobility Measurements on Methylammonium Lead Iodide Perovskite Solar Cells. Appl. Phys. Lett. 2016, 108, 173505.
(22) Li, Y.; Yan, W.; Li, Y.; Wang, W.; Wang, W.; Bian, Z.; Xiao, L.; Gong, Q. Direct Observation of Long Electron-Hole Diffusion Distance beyond 1 Micrometer in $CH_3NH_3PbI_3$ Perovskite Thin Film. Sci. Rep. 2015, 5, 14485.
(23) Xie, F. X.; Su, H.; Mao, J.; Wong, K. S.; Choy, W. C. H. Evolution of Diffusion Length and Trap State Induced by Chloride in Perovskite Solar Cell. J. Phys. Chem. C 2016, 120, 21248−21253.
(24) Leijtens, T.; Stranks, S. D.; Eperon, G. E.; Lindblad, R.; Johansson, E. M. J.; McPherson, I. J.; Rensmo, H.; Ball, J. M.; Lee, M. M.; Snaith, H. J. Electronic Properties of Meso-Superstructured and Planar Organometal Halide Perovskite Films: Charge Trapping, Photodoing, and Carrier Mobility. ACS Nano 2014, 8, 7147−7155.
(25) Oga, H.; Saeki, A.; Ogomi, Y.; Hayase, S.; Seki, S. Improved Understanding of the Electronic and Energetic Landscapes of Perovskite Solar Cells: High Local Charge Carrier Mobility, Reduced Recombination, and Extremely Shallow Traps. J. Am. Chem. Soc. 2014, 136, 13818−13825.
(26) Xu, J.; Buin, A.; Ip, A. H.; Li, W.; Voznyy, O.; Comin, R.; Yuan, M.; Jeon, S.; Ning, Z.; McDowell, J. J.; et al. Perovskite-Fullerene Hybrid Materials Suppress Hysteresis in Planar Diodes. Nat. Commun. 2015, 6, 7081.
(27) Wehrenfennig, C.; Eperon, G. E.; Johnston, M. B.; Snaith, H. J.; Herz, L. M. High Charge Carrier Mobilities and Lifetimes in Organolead Trihalide Perovskites. Adv. Mater. 2014, 26, 1584−1589.

(28) Milot, R. L.; Eperon, G. E.; Snaith, H. J.; Johnston, M. B.; Herz, L. M. Temperature-Dependent Charge-Carrier Dynamics in $CH_3NH_3PbI_3$ Perovskite Thin Films. Adv. Funct. Mater. 2015, 25, 6218−6227.
(29) Hutter, E. M.; Eperon, G. E.; Stranks, S. D.; Savenije, T. J. Charge Carriers in Planar and Meso-Structured Organic-Inorganic Perovskites: Mobilities, Lifetimes, and Concentrations of Trap States. J. Phys. Chem. Lett. 2015, 6, 3082−3090.
(30) Reid, O. G.; Yang, M.; Kopidakis, N.; Zhu, K.; Rumbles, G. Grain-Size-Limited Mobility in Methylammonium Lead Iodide Perovskite Thin Films. ACS Energy Lett. 2016, 1, 561−565.
(31) Kim, D. H.; Park, J.; Li, Z.; Yang, M.; Park, J. S.; Park, I. J.; Kim, J. Y.; Berry, J. J.; Rumbles, G.; Zhu, K. 300% Enhancement of Carrier Mobility in Uniaxial-Oriented Perovskite Films Formed by Topotactic-Oriented Attachment. Adv. Mater. 2017, 29, 1606831.
(32) Guo, Z.; Manser, J. S.; Wan, Y.; Kamat, P. V.; Huang, L. Spatial and Temporal Imaging of Long-Range Charge Transport in Perovskite Thin Films by Ultrafast Microscopy. Nat. Commun. 2015, 6, 7471.
(33) Webber, D.; Clegg, C.; Mason, A. W.; March, S. A.; Hill, I. G.; Hall, K. C. Carrier Diffusion in Thin-Film $CH_3NH_3PbI_3$ Perovskite Measured Using Four-Wave Mixing. Appl. Phys. Lett. 2017, 111, 121905.
(34) Herz, L. M. Charge-Carrier Mobilities in Metal Halide Perovskites: Fundamental Mechanisms and Limits. ACS Energy Lett. 2017, 2, 1539−1548.
(35) Arias, D. H.; Moore, D. T.; van de Lagemaat, J.; Johnson, J. C. Direct Measurements of Carrier Transport in Polycrystalline

Methylammonium Lead Iodide Perovskite Films with Transient Grating Spectroscopy. J. Phys. Chem. Lett. 2018, 9, 5710−5717.
(36) Webber, D.; Clegg, C.; Mason, A. W.; March, S. A.; Hill, I. G.; Hall, K. C. Carrier Diffusion in Thin-Film $CH_3NH_3PbI_3$ Perovskite Measured using Four-wave Mixing. Appl. Phys. Lett. 2017, 111, 121905.
(37) Ciesielski, R.; Scha¨fer, F.; Hartmann, N. F.; Giesbrecht, N.; Bein, T.; Docampo, P.; Hartschuh, A. Grain Boundaries Act as Solid Walls for Charge Carrier Diffusion in Large Crystal MAPI Thin Films. ACS Appl. Mater. Interfaces 2018, 10, 7974−7981.
(38) Yang, M.; Zeng, Y.; Li, Z.; Kim, D. H.; Jiang, C.-S.; van de Lagemaat, J.; Zhu, K. Do Grain Boundaries Dominate Non-Radiative Recombination in $CH_3NH_3PbI_3$ Perovskite Thin Films? Phys. Chem. Chem. Phys. 2017, 19, 5043−5050.
(39) Yang, Y.; Yang, M.; Moore, D. T.; Yan, Y.; Miller, E. M.; Zhu, K.; Beard, M. C. Top and Bottom Surfaces Limit Carrier Lifetime in Lead Iodide Perovskite Films. Nat. Energy 2017, 2, 16207.
(40) Aydin, E.; De Bastiani, M.; De Wolf, S. Defect and Contact Passivation for Perovskite Solar Cells. Adv. Mater. 2019, 31, 1900428.